Manuscript CEJ-D-12-01138-R1

Special issue IMRET-12

Influence of cross-sectional shape on diffusion-free residence time distribution in fully developed laminar Newtonian flow

Sercan Erdogan, Martin Wörner[*]

Karlsruhe Institute of Technology (KIT), Institute for Nuclear and Energy Technologies,

Hermann-von-Helmholtz-Platz 1, 76344 Eggenstein-Leopoldshafen, Germany

[*] Correspondence concerning this article should be address to M. Wörner

E-mail: martin.woerner@kit.edu, Phone +49 721 608 24477, Fax: +49 721 608 24837

Abstract

In this paper, we utilize a recently proposed analytical/semi-analytical method to study the effect of the cross-sectional shape on the diffusion-free residence time distribution (RTD) in fully developed laminar flow of a Newtonian fluid. The diffusion-free RTD is obtained for elliptical channels of arbitrary aspect ratio, for a family of moon-shaped channels, and for an equilateral triangular channel. The non-dimensional RTDs for these channel cross-sections are compared and the influence of the channel shape is found to be rather small. The RTDs can well be approximated by a simple convection model which involves the non-dimensional first appearance time, which represents the ratio between the mean and maximum velocity of the laminar flow, as only parameter. A comparison with recently published results for rectangular channels of arbitrary aspect ratio shows that the one-parameter convection model is unsuited for rectangular channels and a second parameter is required. A first attempt toward the development of such a two-parameter convection model is undertaken, which would then allow predicting the diffusion-free RTD of fully developed laminar flow in straight channels of arbitrary cross-sectional shape.

Nomenclature

a	major semi-axis of elliptical channel (m)
	arc radius of moon-shaped channel (m)
A	channel cross-sectional area (m²)
b	minor semi-axis of elliptical channel (m)
	arc radius of moon-shaped channel (m)
B	parameter of moon-shaped channel, $B = b/(2a)$
C	compactness of channel, $C = P^2/A$
d_h	hydraulic diameter (m)
D	molecular diffusion coefficient (m²/s)
E	differential residence time distribution (1/s)
E_θ	dimensionless differential residence time distribution
F	cumulative residence time distribution
h	height of equilateral triangular channel (m)
K	term defined by Eq. (25)
L	length of channel section (m)
p	parameter in theoretical RTD model
P	channel perimeter (m)
Pe	Peclet number
Q	volumetric flow rate (m³/s)
r	radius in polar coordinate system (m)
R	dimensionless radius in polar coordinate system
Re	Reynolds number
Sc	Schmidt number
t	time (s)
u	cross-sectional profile of axial velocity (m/s)
U_{max}	maximum velocity (m/s)
U_{mean}	mean velocity (m/s)
x	Cartesian co-ordinate, axial (m)
y	Cartesian co-ordinate, cross-sectional (m)
Y	dimensionless Cartesian co-ordinate
z	Cartesian co-ordinate, cross-sectional (m)
Z	dimensionless Cartesian co-ordinate

Greek symbols

β	term defined by Eq. (33)
Γ	gamma function
θ	dimensionless residence time
θ_{F}	dimensionless first appearance time
λ	dimensionless parameter, $\lambda = u / U_{\text{max}} = \theta / \theta_{\text{F}}$
μ	dynamic viscosity (Pa s)
ν	kinematic viscosity (m^2/s)
Π	pressure (Pa)
τ	mean residence time (s)
φ	angle in polar coordinate system
χ	aspect ratio

Subscripts

c	critical value
F	first appearance
max	maximum value
mean	mean value

Abbreviations

RTD	residence time distribution

1. Introduction

Technical applications with fluid flow through circular channels are ubiquitous in the macro-scale, but are rather exceptional in the micro-scale. For manufacturing reasons, microchannels are often not circular but rectangular, trapezoidal, triangular, elliptical or of irregular type. Owing to the small dimensions, the flow in microchannels and microreactors is predominantly laminar. In general, the axial velocity gradually changes from zero at the boundaries to a maximum value in the channel center. Associated with this velocity variation in the direction transverse to the mean flow is a spreading of dissolved matter along the flow direction. This phenomenon, which was first studied by Taylor [1] and Aris [2], is commonly denoted as dispersion and often quantified in terms of the residence time distribution (RTD) [3, 4]. When the time scale of tracer diffusion is large as compared to the convective time scale (i.e. the Peclet number is low), the spreading of the sample is effectively diffusive (Taylor-Aris dispersion). The effects of cross-sectional shape and aspect ratio of shallow microchannels on Taylor dispersion was investigated in several papers [5-9]. Theoretical studies showed that dispersion is in most cases controlled by the width of the cross-section rather than by the much thinner height [5, 6], in agreement with experiments [7]. Simple formulas permit a quantitative evaluation of dispersion for most shallow cross-sectional shapes in the diffusive Taylor regime [6].

In liquids, diffusion coefficients are rather small and the Schmidt number $Sc = v / D$ is typically of order 1000. Thus, even small values of the Reynolds number $Re = d_{\mathrm{h}} U_{\mathrm{mean}} / v$ may be associated with high Peclet numbers $Pe = Sc \cdot Re$ so that convection dominates over diffusion and the RTD is affected by the non-uniform velocity distribution of the laminar flow (at least in channels that are not exceptionally long). Under these conditions, accurate measurement of the RTD in microchannels is very difficult because the tracer injection and detection must be flux-weighted (i.e. be proportional to the local fluid velocity within the channel cross-section). Many published experimental results in laminar flow deal with concentration responses that are not RTDs in a strict sense because they are not weighted by the local fluid velocity. In the limit of negligible diffusion, the RTD is fully determined by the non-uniform velocity profile alone and analytical studies can provide some insight. Explicit

analytical forms of the diffusion-free RTD in laminar flows are, however, known only for very few channel shapes, where the velocity profile depends on one co-ordinate only, namely circular pipe flow [3, 10], Poiseuille and Couette flow between two parallel plates, and falling film flow [11]. In contrast to Taylor-Aris dispersion, a systematic study on the effect of the cross-sectional shape on the diffusion-free RTD in laminar flows is missing. Recently, an analytical method was proposed by one of the authors which allows (under certain conditions) determining the diffusion-free RTD of fully developed laminar flow in straight channels where the velocity profile depends on *two* co-ordinates [12]. The method was used to determine approximate RTDs for rectangular channels of arbitrary aspect ratio. In the present paper, we utilize this technique for determining the diffusion-free RTD of laminar Newtonian flow in elliptical channels of arbitrary aspect ratio, in an equilateral triangular channel, and in a family of moon-shaped channels. While moon-shaped channels may not be manufactured in practice, they are attractive in the present context since they allow a significant variation of the channel shape by changing a single geometric parameter. To the best of our knowledge, the diffusion-free RTDs for all these channels have not been determined so far.

For laminar flows, the diffusion-free RTD is rather wide with long tails and the simple dispersed plug flow model originating from Taylor-Aris theory is not adaptable for small Reynolds number [13]. For reaction engineering, a narrow RTD and plug flow behavior are beneficial and the wide RTD of laminar flow is a certain drawback. Highly welcome for engineering practice would be a model which allows estimating the microreactor RTD under very small or negligible diffusion from the laminar flow RTD in a straight microchannel. For this purpose, the diffusion-free RTDs for various channel cross-sections obtained in this paper are compared and a first attempt is made to develop a general RTD model for laminar flow in channels of arbitrary shape.

In the sequel, we give in Section 2 some basic definitions and describe the general procedure for computing the RTD from the laminar velocity profile. In Section 3, we present the results for the different channel types and provide a detailed discussion. In Section 4 we present the conclusions.

6

2. Theory

In this section we introduce some basic definitions, explain the method for evaluating the diffusion-free RTD from the laminar velocity profile and give an analytical model for the RTD of laminar flows that will be used for fitting purposes.

2.1. Basic definitions

The differential RTD, $E(t)$, of a chemical reactor is a distribution function that describes the amount of time that fluid elements spend inside the reactor [4, 14]. For comparing different reactors the non-dimensional RTD curve

$$E_\theta(\theta) \equiv \tau \cdot E(t) \tag{1}$$

is useful, which is a function of a dimensionless time $\theta \equiv t / \tau$. Here, $\tau = \int_0^\infty t E(t) \mathrm{d}t$ denotes the mean residence time. Equation (2) relates the non-dimensional differential RTD $E_\theta(\theta)$ with the cumulative RTD $F(\theta)$

$$E(\theta) = \frac{\mathrm{d}F(\theta)}{\mathrm{d}\theta} \tag{2}$$

2.2. Procedure for evaluation of the diffusion-free RTD in laminar flow

In the absence of diffusion, the cumulative RTD due to pure convective transport is given by [15]

$$F(\theta) = \frac{Q(\theta)}{Q_{\mathrm{total}}} \tag{3}$$

Here, $Q(\theta)$ is the volumetric flow rate associated with a residence time θ or lower, and Q_{total} is the total volumetric flow rate. The non-dimensional residence time of the fastest fluid elements is commonly denoted as first-appearance or break-through time θ_{F}. For fully developed laminar flow in a straight channel it is given by

$$\theta_{\mathrm{F}} = \frac{U_{\mathrm{mean}}}{U_{\mathrm{max}}} \tag{4}$$

where U_{mean} and U_{max} denote the mean and maximum axial velocity, respectively. For our analysis we assume that the profile of the axial velocity is monotonic and increases from zero at the walls (no-slip condition) to a maximum U_{max} located at a unique position within the channel cross-section.

For an axial channel section of length L the non-dimensional residence time of fluid elements moving with velocity $u_\lambda = \lambda U_{max}$ is

$$\theta = \frac{t}{\tau} = \frac{L/\lambda U_{max}}{L/U_{mean}} = \frac{1}{\lambda} \frac{U_{mean}}{U_{max}} = \frac{\theta_F}{\lambda} \tag{5}$$

where $0 < \lambda \leq 1$. The volumetric flow rate associated with a certain value of λ is

$$Q = \iint_{A_\lambda} u \, dA \tag{6}$$

where A_λ denotes the area within the channel cross-section where $u/U_{max} \geq \lambda$. With $Q_{total} = A U_{mean} = A \theta_F U_{max}$ we obtain from Eqs. (3) and (6) the result

$$F(\theta) = \frac{1}{A\theta_F} \iint_{A_\lambda} \frac{u}{U_{max}} \, dA \tag{7}$$

In Section 3 we will utilize Eq. (7) to evaluate the RTD for laminar flow in channels of various shapes. We remark that in the absence of diffusion and turbulence, the RTD is not a probabilistic but a fully deterministic quantity.

2.3. Generalized convection model

Some of the RTDs in Section 3 will be obtained in discrete form. For practical purposes it is useful to approximate the discrete RTD by a continuous function. In this paper we will employ the model

$$E_\theta(\theta) = \begin{cases} 0 & \text{for} \quad \theta < \theta_F \\ \dfrac{\Gamma\left(1 + (p-2)\theta_F^{-1}\right)}{\Gamma(p-1)\Gamma\left((p-2)(\theta_F^{-1}-1)\right)} \dfrac{\theta_F^{p-1}}{\theta^p}\left(1 - \dfrac{\theta_F}{\theta}\right)^{(p-2)(\theta_F^{-1}-1)-1} & \text{for} \quad \theta \geq \theta_F \end{cases} \tag{8}$$

which was recently proposed for fitting of laminar RTD curves [12]. Here, Γ denotes the gamma function. The respective cumulative RTD involves the Gauss hypergeometric function and can be found in [12]. Since θ_F is assumed to be known from the ratio of mean to maximum velocity, only p

remains as free parameter. In Section 3 we will determine p by minimizing the difference between a given set of discrete RTD values and model (8) by least square fitting and denote this value by p_{L^2}.

An important feature of the RTD in Eq. (8) is that for $p < p_{crit} = 2 + (\theta_F^{-1} - 1)^{-1}$ the value $E_\theta(\theta = \theta_F)$ is infinite whereas it is finite for $p \geq p_{crit}$. For $p = p_{crit}$ the RTD in Eq. (8) simplifies to the form

$$E_\theta = \begin{cases} 0 & \text{for} \quad \theta < \theta_F \\ \dfrac{1}{1-\theta_F} \dfrac{1}{\theta} \left(\dfrac{\theta_F}{\theta} \right)^{\frac{1}{1-\theta_F}} & \text{for} \quad \theta \geq \theta_F \end{cases} \tag{9}$$

which was first proposed by Levenspiel [16] and is here denoted as generalized one-parameter convection model. In the sequel we will for simplicity only give RTD formulas for the branch $\theta \geq \theta_F$ while it is understood that $E_\theta = F_\theta = 0$ for $0 \leq \theta < \theta_F$.

3. Diffusion-free RTD for different channel cross-sections

3.1. Elliptical channel

We consider an elliptical channel with major and minor semi-axes a and b as shown in Fig. 1 a). We denote the aspect ratio by $\chi \equiv b/a$ and define $Y \equiv y/b$ and $Z \equiv z/a$. Then, for a Newtonian fluid the fully developed laminar velocity profile can be written as [17, 18]

$$u(Y,Z) = U_{max}(1 - Y^2 - Z^2) \tag{10}$$

The mean value of this velocity profile is $U_{mean} = U_{max}/2$. Thus, by Eq. (4) the non-dimensional first-appearance time is $\theta_F = 0.5$, independent from χ.

The position of isolines where the velocity has a constant value $u = \lambda U_{max}$ is given by

$$Z_{\lambda+} = -Z_{\lambda-} = \sqrt{1 - \lambda - Y^2} \tag{11}$$

For $Z_\lambda = 0$ we obtain $Y_{max,\lambda} = -Y_{min,\lambda} = \sqrt{1 - \lambda}$. Taking into account the symmetry of the problem, we obtain from Eq. (7) with $A = \pi ab$ and $\theta_F = 0.5$ the result

9

$$F(\theta) = \frac{2}{\pi} \int\limits_{Y_{\min,\lambda}}^{Y_{\max,\lambda}} \int\limits_{Z_{\lambda-}}^{Z_{\lambda+}} \left(1 - Y^2 - Z^2\right) dZ dY = \frac{8}{\pi} \int\limits_{0}^{Y_{\max,\lambda}} Z_{\lambda+} \left(1 - Y^2 - \frac{1}{3} Z_{\lambda+}^2\right) dY$$

$$= \frac{8}{\pi} \int\limits_{0}^{\sqrt{1-\lambda}} \sqrt{1 - \lambda - Y^2} \left(\frac{2+\lambda}{3} - \frac{2}{3} Y^2\right) dY$$

(12)

Integration yields

$$F(\theta) = \frac{2}{3\pi} \left[Y\sqrt{1-\lambda-Y^2}(5+\lambda-2Y^2) - 3(\lambda^2-1)\tan^{-1}\left(\frac{Y}{\sqrt{1-\lambda-Y^2}}\right) \right]_{Y=0}^{Y=\sqrt{1-\lambda}}$$

$$= 1 - \lambda^2 = 1 - \frac{1}{4\theta^2}$$

(13)

so that we finally obtain for the differential RTD the result

$$E(\theta) = \frac{1}{2\theta^3}$$

(14)

Thus, regardless of χ, the RTD of any elliptical channel is identical with the RTD of a circular channel. We remark that for $\theta_F = 0.5$ and $p = 3$ Eqs. (8), (9) and (14) are all identical.

3.2. Equilateral triangular channel

We consider an equilateral triangular channel with side length a and height $h = a\sqrt{3}/2$ as displayed in Fig. 1 b). We define $Y \equiv y/h$ and $Z \equiv z/h$. Then, the fully developed laminar velocity profile is given by [17, 19]

$$u(Y,Z) = \frac{27}{4} U_{\max} \left(1 - Y\right)\left(Y^2 - 3Z^2\right)$$

(15)

The mean value of this velocity profile is $U_{\text{mean}} = (9/20)U_{\max}$ so that $\theta_F = 0.45$. The location of velocity isolines with value $u = \lambda U_{\max}$ is defined by

$$Z_{\lambda+} = -Z_{\lambda-} = \frac{1}{\sqrt{3}} \sqrt{Y^2 - \frac{4}{27}\frac{\lambda}{1-Y}}$$

(16)

The determination of $Y_{\min,\lambda}$ and $Y_{\max,\lambda}$ leads to a cubic equation. The two roots of interest here are

$$Y_{\min,\lambda} = \frac{1}{3} + \frac{2}{3}\cos\left(\frac{4\pi}{3} + \frac{1}{3}\cos^{-1}(1-2\lambda)\right)$$

(17)

$$Y_{\max,\lambda} = \frac{1}{3} + \frac{2}{3}\cos\left(\frac{1}{3}\cos^{-1}(1-2\lambda)\right)$$

(18)

From Eq. (7) we obtain with $A = h^2 / \sqrt{3}$ the result

$$F(\theta) = 15\sqrt{3} \int_{Y_{\min,\lambda}}^{Y_{\max,\lambda}} \int_{Z_{\lambda-}}^{Z_{\lambda+}} (1-Y)(Y^2 - 3Z^2)\,dZdY = 30\sqrt{3}\int_{Y_{\min,\lambda}}^{Y_{\max,\lambda}} Z_{\lambda+}(1-Y)(Y^2 - Z_{\lambda+}^2)\,dY$$

(19)

$$= 30\int_{Y_{\min,\lambda}}^{Y_{\max,\lambda}} (1-Y)\left(\frac{2}{3}Y^2 + \frac{4}{81}\frac{\lambda}{1-Y}\right)\sqrt{Y^2 - \frac{4}{27}\frac{\lambda}{1-Y}}\,dY$$

Since this integration cannot be performed analytically, we evaluated it numerically with Mathematica for a set of discrete values $\lambda_i = \theta_F / \theta_i = i\Delta\lambda$. Here, and in the sequel, we used $\Delta\lambda = 0.01$ and $i = 1,...,100$. From the discrete cumulative RTD the discrete differential RTD is computed as

$$E(\theta_{i+1/2}) = \frac{F_{i+1} - F_i}{\theta_{i+1} - \theta_i}$$

(20)

where $\theta_{i+1/2} = (\theta_i + \theta_{i+1})/2$. The respective differential RTD of the equilateral triangular channel is displayed in Fig. 2. Fitting of this discrete semi-analytical RTD curve by the generalized model of Eq. (8) yields $p_{L^2} = 2.831$. As shown in Fig. 2, the agreement between the semi-analytical and the fitted RTD is very good.

3.3. Moon-shaped channel

3.3.1. Geometric parameters

Shah and London [18] introduced a moon-shaped channel formed by two circular arcs with radiuses a and b as displayed in Fig. 1 c). We define $R \equiv r/(2a)$, $B \equiv b/(2a)$ where $0 \le B < 1$. Depending on the parameter B quite different channel cross-sections can be obtained. The cross-sectional shape is circular for $B = 0$, moon-like for $B > 0$ and becomes slit-like in the limit $B \to 1$, see Fig. 1 d). The area and perimeter of the moon-shaped channel are given by

$$A = 2a^2\left[(1-2B^2)\cos^{-1}B + B\sqrt{1-B^2}\right]$$

(21)

$$P = 4a(1+B)\cos^{-1}B$$

(22)

3.3.2. Velocity profile

The laminar Poiseuille velocity profile of the moon-shaped channel is [18]

$$u(r,\varphi) = \frac{c_1}{4}(r^2 - b^2)\left(1 - \frac{2a\cos\varphi}{r}\right)$$
(23)

where $c_1 = -\mu^{-1}(\partial\Pi/\partial x)$ with Π denoting the pressure. Here, we rewrite this profile in the form

$$u(R,\varphi) = U_{max}K^{-1}(R^2 - B^2)(1 - R^{-1}\cos\varphi)$$
(24)

where

$$K = (R^2_{U,max} - B^2)(1 - R^{-1}_{U,max})$$
(25)

The variable $R_{U,max}$ denotes the radius where the velocity has its maximum value so that $u(R_{U,max}, 0) = U_{max}$. This position is a function of B and is given by

$$R_{U,max} = \frac{1}{6}\left(1 + \sqrt[3]{1 + 54B\left(B + \sqrt{\frac{1}{27} + B^2}\right)} + \sqrt[3]{1 + 54B\left(B - \sqrt{\frac{1}{27} + B^2}\right)}\right)$$
(26)

By evaluating the mean value of velocity profile (24) we obtain for the non-dimensional first-appearance time of the moon-shaped channel the result

$$\theta_F = \frac{1}{8}\frac{B(1 + 14B^2)\sqrt{1 - B^2} - \left[8B^2(1 + B^2) - 1\right]\cos^{-1}B}{(R^2_{U,max} - B^2)(R^{-1}_{U,max} - 1)\left[B\sqrt{1 - B^2} + \left(1 - 2B^2\right)\cos^{-1}B\right]}$$
(27)

In Fig. 3 we show $R_{U,max}$ and θ_F as function of B. We see that the value of θ_F is not very sensitive with respect to B and is within the range $0.45 < \theta_F \leq 0.5$. Thus, the significant change of the channel shape that is associated with the variation of B in the range $0 \leq B < 1$ results only in a rather small variation of the first appearance time.

3.3.3. Velocity isolines

By introducing $u = \lambda U_{max}$ into Eq. (24) we obtain as condition for the velocity isolines the relation

$$\lambda = K^{-1}(R^2 - B^2)\left(1 - \frac{\cos\varphi}{R}\right)$$
(28)

so that

$$\varphi_\lambda(R,\lambda) = \cos^{-1}\left[R\left(1 - \frac{\lambda K}{R^2 - B^2}\right)\right] \qquad (29)$$

Determining the minimum and maximum value of R for the velocity isolines requires solution of the cubic equation

$$R^3 - R^2 \cos\varphi - (B^2 + \lambda K)R + B^2 \cos\varphi = 0 \qquad (30)$$

which follows from Eq. (28). The two roots of Eq. (30) which are of interest here are

$$R_{\max,\lambda} = \frac{1}{3}\cos\varphi + \frac{2}{3}\sqrt{3B^2 + 3\lambda K + \cos^2\varphi}\,\cos\left(\frac{\beta}{3}\right) \qquad (31)$$

$$R_{\min,\lambda} = \frac{1}{3}\cos\varphi + \frac{2}{3}\sqrt{3B^2 + 3\lambda K + \cos^2\varphi}\,\cos\left(\frac{\beta}{3} + \frac{4\pi}{3}\right) \qquad (32)$$

where

$$\beta = \arccos\left(-\frac{1}{2}\frac{18B^2 - 2\cos^2\varphi - 9\lambda K}{(3B^2 + \cos^2\varphi + 3\lambda K)^{3/2}}\cos\varphi\right) \qquad (33)$$

In Fig. 4 a) we plot the velocity isolines for $B = 0.5$ and four different values of λ. The left branch of each isoline results from $R_{\min,\lambda}$ and the right one from $R_{\max,\lambda}$. In Fig. 4 b) we display the axial velocity as height function above the $y - z$ plane in the area enclosed by the isolines for $B = 0.3$ and $\lambda = 0.5$. In this 3D representation, the enclosed volume corresponds to the volumetric flow rate $Q(\theta)$ which must be determined in order to compute the cumulative RTD according to Eq. (7) for the specific value $\theta = \theta_F / \lambda = 2\theta_F$.

For the cumulative RTD of the moon-shaped channel we obtain the relation

$$\begin{aligned}
F(\theta) &= \frac{2}{A\theta_F}\int_{R_{\min,\lambda}}^{R_{\max,\lambda}}\int_0^{\varphi_\lambda} K^{-1}(R^2 - B^2)(1 - R^{-1}\cos\varphi)4a^2 R\,\mathrm{d}\varphi\,\mathrm{d}R \\
&= \frac{8a^2}{A\theta_F}\int_{R_{\min,\lambda}}^{R_{\max,\lambda}} K^{-1}(R^2 - B^2)(R\varphi_\lambda - \sin\varphi_\lambda)\,\mathrm{d}R
\end{aligned} \qquad (34)$$

Introducing Eq. (29) in Eq. (34) and recognizing the relation

13

$$\sin \varphi_\lambda = \sin \left[\cos^{-1} \left(R - \frac{R \lambda K}{R^2 - B^2} \right) \right] = \sqrt{1 - \left(R - \frac{R \lambda K}{R^2 - B^2} \right)^2} \tag{35}$$

yields

$$F(\theta) = \frac{8 a^2}{A \theta_{\mathrm{F}}} \int_{R_{\min,\lambda}}^{R_{\max,\lambda}} \frac{R^2 - B^2}{K} \left[R \cos^{-1} \left(R - \frac{R \lambda K}{R^2 - B^2} \right) - \sqrt{1 - \left(R - \frac{R \lambda K}{R^2 - B^2} \right)^2} \right] \mathrm{d}R \tag{36}$$

where A and θ_{F} are given by Eq. (21) and Eq. (27), respectively. Again, an analytical integration is not possible. Therefore, we evaluated for a given value of B integral (36) numerically with Mathematica for a discrete set of values $\lambda_i = i \Delta \lambda$. Subsequently, the differential RTD was computed by means of Eq. (20).

In Fig. 5 we show the discrete differential RTD for five different values of B, namely 0, 0.25, 0.5, 0.75, and 0.99. Though the channel shapes are quite different, the difference of the RTDs is rather small. This result is consistent with the rather low variation of θ_{F} noted previously, cf. Fig. 2. To obtain a continuous approximation, we again fitted for all cases with $B > 0$ the discrete RTD by the generalized RTD of Eq. (8). The respective values of p_{L^2} are listed in Tab. 1 together with those for p_{crit}. A comparison shows that both values are almost identical. This also holds for the equilateral triangular channel. We also compared for $B = 0.5$ the semi-analytical RTD with Eq. (8) for $p = p_{L^2} = 2.896$ and $p = p_{\mathrm{crit}} = 2.893$ and found that the curves are almost indistinguishable.

3.4. Effect of cross-sectional shape

To investigate the effect of the cross-sectional shape on the diffusion-free RTD, we display in Fig. 6 the values of p as function of θ_{F} for various channel types. Shown are the present results for elliptical channels, the equilateral triangular channel, and four different moon-shaped channels (with different values of B). Also shown are results from [12] for rectangular channels with different aspect ratio χ. The first appearance time of the rectangular channels was computed from Eq. (37)

$$\theta_F = \frac{2}{3} \left(1 + 0.546688 \chi + 1.552013 \chi^2 - 4.059427 \chi^3 + 3.214927 \chi^4 - 0.857313 \chi^5 \right)^{-1} \tag{37}$$

This correlation was proposed by Spiga and Morini [20] who determined exact values of U_{max}/U_{mean} for ten distinct aspect ratios in the range $0 \leq \chi \leq 1$ and fitted these data by Eq. (37) with an accuracy of 0.06%. For the parameter p in Eq. (8) the relation

$$p(\chi) = 3 - 0.4\chi + 0.2\chi^2 \tag{38}$$

was proposed in [12]. For a planar channel it is $\chi = 0$; then, the latter two correlations yield $\theta_F = 2/3$ and $p = 3$ so that the exact RTD is recovered from Eq. (8). For all other aspect ratios, the RTD curve resulting from Eqs. (8), (37) and (38) must be considered as approximate.

From Fig. 6 we can observe that the data for the spherical, elliptical, moon-shaped and equilateral triangular channels all collapse to a single curve which is rather well represented by the generalized one-parameter convection model given by Eq. (9). In this model, the RTD is a unique function of the first appearance time θ_F. Fig. 6 also shows that for rectangular channels a completely different curve is obtained and the generalized one-parameter convection model is not appropriate. It is evident that moon-shaped and rectangular channels may have the same value of $\theta_F = U_{mean}/U_{max}$ while the value of p is different. In rectangular channels, the value of p is always notably smaller than p_{crit}. As a consequence the last exponent in Eq. (8) is never zero as it is the case with the generalized one-parameter convection model in Eq. (9).

Since the data for the various channel shapes in Fig. 6 do not collapse to a single curve, and because for the same value of θ_F the value of p may differ, we conclude that θ_F alone is not sufficient to determine the RTD for channels of arbitrary shape. Therefore, for the purpose of generalization, a relation is required which connects p in Eq. (8) not only to θ_F but to a further dimensionless parameter which accounts in some way for the channel shape. A suitable parameter could be the compactness $C = P^2/A$ which is used in [21] to account for the shape dependence of the hydraulic resistance in microchannels. The value of C is $4\pi \approx 12.57$ for a circular channel, 16 for a square channel and $12\sqrt{3} \approx 20.78$ for a equilateral triangular channel. For rectangular and elliptical channels, the value of C depends on the aspect ratio and tends to infinity in the limit $\chi \to 0$. We displayed the values of p for various channel cross-sections and aspect ratios as function of θ_F and

C and found that with increase of C the value of p decreases for moon-shaped channels but increases for rectangular channels. This indicates that the compactness is not useful in the present context. Instead, a model for predicting the diffusion-free RTD in laminar flow from the channel shape must be based on another appropriate but yet unknown dimensionless parameter. The determination of such a parameter will be a future task for us.

3.5. *Range of validity and applicability of diffusion-free RTD model*

The results obtained in this paper for the diffusion-free RTD may find practical application, provided the assumptions of fully developed laminar flow and negligible influence of molecular diffusion are fulfilled. A detailed assessment of these terms for rectangular channels was performed in [12] where mathematical criteria for the following conditions were derived: i) laminar flow, ii) fully developed flow and negligible entrance effects, iii) negligible transversal diffusion, and iv) negligible longitudinal diffusion. In a diagram where the ratio of channel length to channel diameter is plotted over the Reynolds number, these four conditions define a finite region where the theory is valid. The size of this region depends on the Schmidt number. In practice, the diffusion-free RTD theory is never valid for gas flows where the Schmidt number is of order unity. It can, however, be a reasonable approximation for liquid flows where the Schmidt number is typically of order 1000. For the impact of the entrance region on the RTD in laminar flow through tubes and ducts the interested reader is referred to a recent investigation by Ham et al. [22]. Another limitation of the present model is its restriction to straight channels. Many long microchannels or microreactors are made of meandering or zig-zag channels and the Dean vortices at the bends may have a notable effect on the RTD.

4. Conclusions

In this paper we computed the diffusion-free RTD in fully developed laminar Newtonian flow through straight channels of various cross-sectional shapes from the known velocity profiles. In elliptical channels, the diffusion-free RTD is identical to that in a circular channel, regardless of the aspect ratio. For the family of moon-shaped channels, the RTD slightly broadens as the shape

16

changes from circular to slit-like. Overall, the influence of the cross-sectional shape on the diffusion-free RTD in straight channels is surprisingly small.

The non-dimensional diffusion-free RTDs of channels with less than four corners (spherical/elliptical, moon-shaped, equilateral triangular) is reasonably well described by the generalized convection model of Eq. (9) which involves the non-dimensional first appearance time θ_F as only parameter. Thus, for channels whose shape is similar to the shape of any channel from the family of moon-shaped channels, the one-parameter convection model of Eq. (9) provides a reasonable good estimation for the diffusion-free RTD. The respective non-dimensional first appearance time θ_F, which is given by the ratio between mean and maximum velocity, can easily be determined numerically.

A comparison with recent results for rectangular channels of arbitrary aspect ratio shows that the one-parameter convection model is unsuited for rectangular channels. The diffusion-free RTD of rectangular channels is instead well described by the generalized two-parameter convection model of Eq. (8) which includes the one-parameter convection model as special case. Correlating the second parameter p of this model with an appropriate parameter that accounts for the channels cross-sectional shape remains an open task; the channel compactness appeared unsuited in this context. Identifying an appropriate non-dimensional shape-characterizing parameter, with which p could be successfully correlated, would yield a closed model that would allow estimating the diffusion-free RTD of fully developed laminar flow in straight channels of arbitrary cross-sectional shape.

In practice, the generalized one- and two-parameter convection models may be used to estimate the RTD of liquid flows with high Schmidt number provided the length-to-diameter ratio of the channel is, for a given Reynolds number, on one-hand side sufficiently large so that the flow is fully developed and entrance effects are small, and at the same time not too large so that transversal diffusion is still negligible.

References

[1] G. Taylor, Dispersion of Soluble Matter in Solvent Flowing Slowly through a Tube, Proc R Soc Lon Ser-A, 219 (1953) 186-203.

[2] R. Aris, On the Dispersion of a Solute in a Fluid Flowing through a Tube, Proc R Soc Lon Ser-A, 235 (1956) 67-77.

[3] P.V. Danckwerts, Continuous Flow Systems - Distribution of Residence Times, Chem Eng Sci, 2 (1953) 1-13.

[4] O. Levenspiel, Chemical reaction engineering, 3rd ed., John Wiley & Sons, Hoboken, NJ, 1999.

[5] D.C. Guell, R.G. Cox, H. Brenner, Taylor Dispersion in Conduits of Large Aspect Ratio, Chem Eng Commun, 58 (1987) 231-244.

[6] A. Ajdari, N. Bontoux, H.A. Stone, Hydrodynamic dispersion in shallow mirochannels: the effect of cross-sectional shape, Anal Chem, 78 (2006) 387-392.

[7] N. Bontoux, A. Pepin, Y. Chen, A. Ajdari, H.A. Stone, Experimental characterization of hydrodynamic dispersion in shallow microchannels, Lab Chip, 6 (2006) 930-935.

[8] A. Vikhansky, Taylor dispersion in shallow micro-channels: aspect ratio effect, Microfluid Nanofluid, 7 (2009) 91-95.

[9] J. Aubin, L. Prat, C. Xuereb, C. Gourdon, Effect of microchannel aspect ratio on residence time distributions and the axial dispersion coefficient, Chemical Engineering and Processing: Process Intensification, 48 (2009) 554-559.

[10] R.C.L. Bosworth, Distribution of reaction times for laminar flow in cylindrical reactors, Philosophical Magazine Series 7, 39 (1948) 847-862.

[11] O. Levenspiel, B.W. Lai, C.Y. Chatlynne, Tracer curves and the residence time distribution, Chem Eng Sci, 25 (1970) 1611-1613.

[12] M. Wörner, Approximate residence time distribution of fully develop laminar flow in a straight rectangular channel, Chem Eng Sci, 65 (2010) 3499-3507.

[13] C. Andre, B. Boissier, L. Fillaudeau, Residence time distribution in tubular Joule effect heaters with and without geometric modifications, Chem Eng Technol, 30 (2007) 33-40.

[14] E.B. Nauman, Residence time theory, Ind Eng Chem Res, 47 (2008) 3752-3766.

[15] O. Wein, J. Ulbrecht, Residence time distribution in laminar flow systems. II: Non-Newtonian tubular flow, Collect Czech Chem C, 37 (1972) 3240-3259.

[16] O. Levenspiel, The chemical reactor omnibook, 2nd ed., Oregon State University Book Stores, 1989.

[17] H.L. Dryden, F.D. Murnaghan, H. Bateman, Report of the Committee on Hydrodynamics, Division of Physical Sciences National Research Council, National Research Council of the National Academy of Sciences, Washington, DC, 1932.

[18] R.K. Shah, A.L. London, Laminar flow forced convection in ducts: a source book for compact heat exchanger analytical data, Academic Press, New York, 1978.

[19] R. Berker, Intégration des équations du mouvement d'un fluide visqueux incompressible, in: S. Flügge, C. Truesdell (Eds.) Handbuch der Physik, Band VIII/2 Strömungsmechanik II, Springer-Verlag, Berlin, 1963, pp. 1-384.

[20] M. Spiga, G.L. Morini, A Symmetrical Solution for Velocity Profile in Laminar-Flow through Rectangular Ducts, Int Commun Heat Mass, 21 (1994) 469-475.

[21] N.A. Mortensen, F. Okkels, H. Bruus, Reexamination of Hagen-Poiseuille flow: Shape dependence of the hydraulic resistance in microchannels, Phys Rev E, 71 (2005).

[22] J.H. Ham, R. Lohse, B. Platzer, Modeling of the Laminar Flow in the Entrance Region of Tubes and Ducts and its Impact on the Residence Time Distribution, Chem-Ing-Tech, 83 (2011) 1245-1255.

Figure captions

Fig. 1: Sketch of channel shapes considered in this paper: a) elliptical channel, b) equilateral triangular channel, c) general moon-shaped channel, d) moon-shaped channel for different values of B.

Fig. 2: Differential RTD of equilateral triangular channel. Comparison of discrete semi-analytical RTD with generalized two-parameter convection model.

Fig. 3: Position of velocity maximum $R_{U,\max}$ and first appearance time θ_{F} of moon-shaped channel as function of B.

Fig. 4: a) Channel shape (thick solid lines) and position of velocity isolines (thin solid and dashed lines) for $B = 0.5$. The values of the isolines correspond to $\lambda = u/U_{\max} = 0.25, 0.5, 0.75, 0.9$ (from outermost to innermost). The solid part of each isoline corresponds to $R_{\max,\lambda}$ and the dashed part to $R_{\min,\lambda}$ as given by Eq. (31) and Eq. (32), respectively. b) Height function representation of the axial velocity u over the $y-z$ plane for a moon-shaped channel with $B = 0.3$ within area A_{λ} for $\lambda = 0.5$. The volume below the surface corresponds to the volumetric flow rate $Q(\theta)$ for the specific residence time $\theta = \theta_{\mathrm{F}}/\lambda = 2\theta_{\mathrm{F}}$.

Fig. 5: Differential RTD of moon-shaped channels for $B = 0, 0.25, 0.5, 0.75, 0.99$ in linear and double-log representation. The corresponding channel shapes are shown in Fig. 1 d).
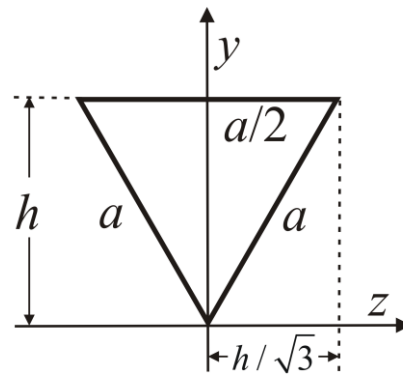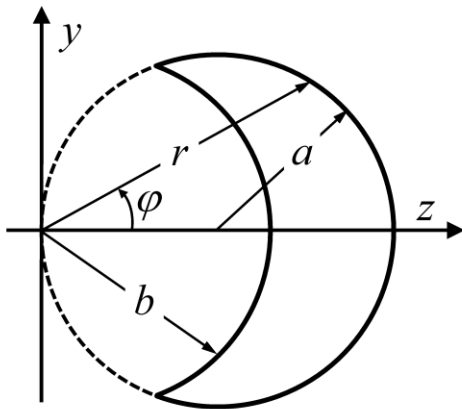
Fig. 6: Parameter p of the generalized two-parameter convection model from Eq. (8) as function of the first appearance time θ_{F} for different channel shapes (data for rectangular channels are from [12]). The dashed line corresponds to $p = p_{\mathrm{crit}} = 2 + (\theta_{\mathrm{F}}^{-1} - 1)^{-1}$ where the two-parameter convection model reduces to the one-parameter convection model of Eq. (9).
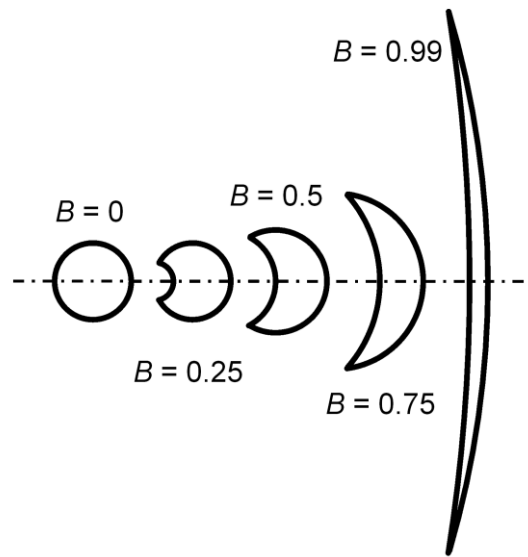
Figures

Fig. 1: Sketch of channel shapes considered in this paper: a) elliptical channel, b) equilateral triangular channel, c) general moon-shaped channel, d) moon-shaped channel for different values of B
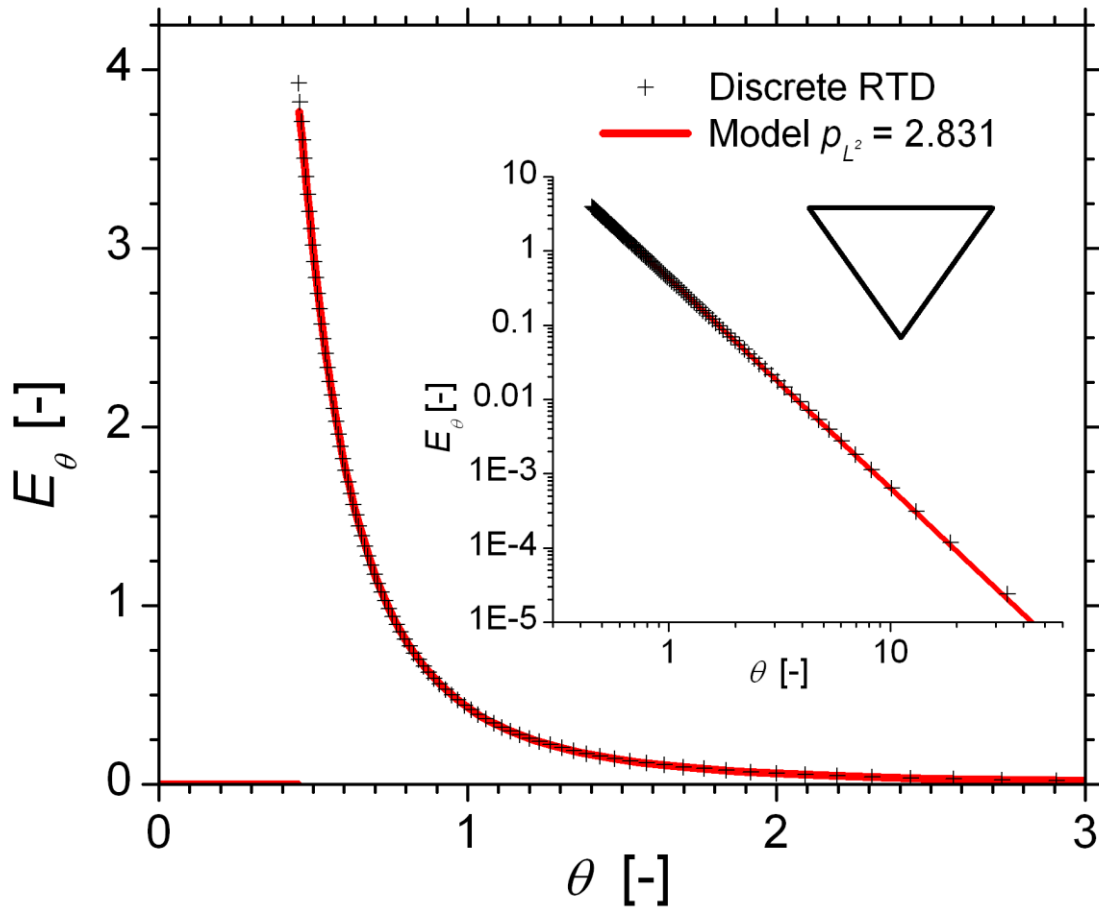
Fig. 2: Differential RTD of equilateral triangular channel. Comparison of discrete semi-analytical RTD with generalized two-parameter convection model.
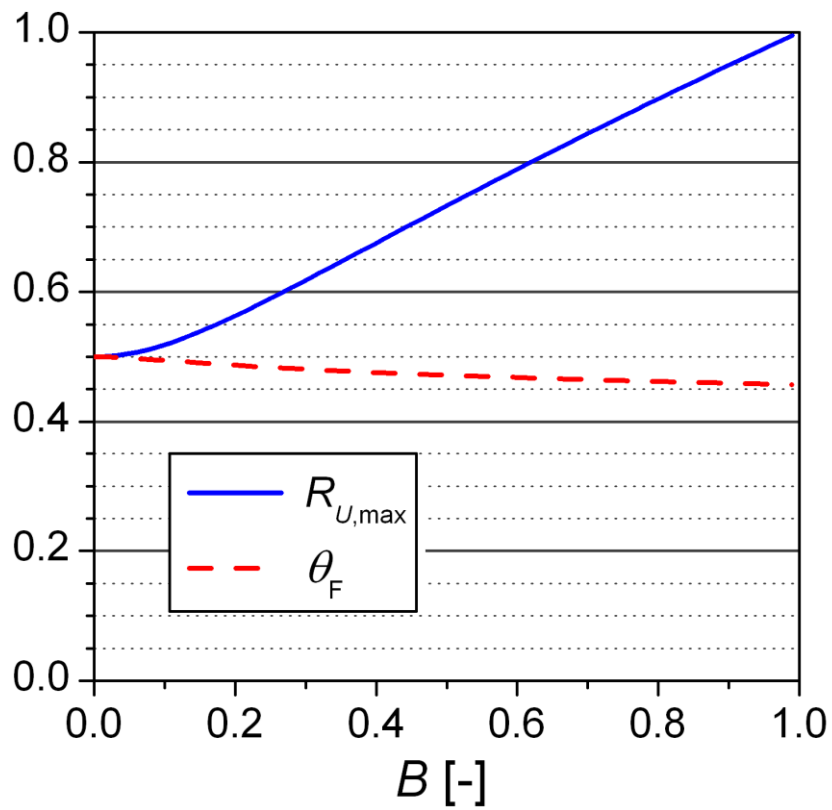
Fig. 3: Position of velocity maximum $R_{U,\max}$ and first appearance time θ_{F} of moon-shaped channel as function of B.
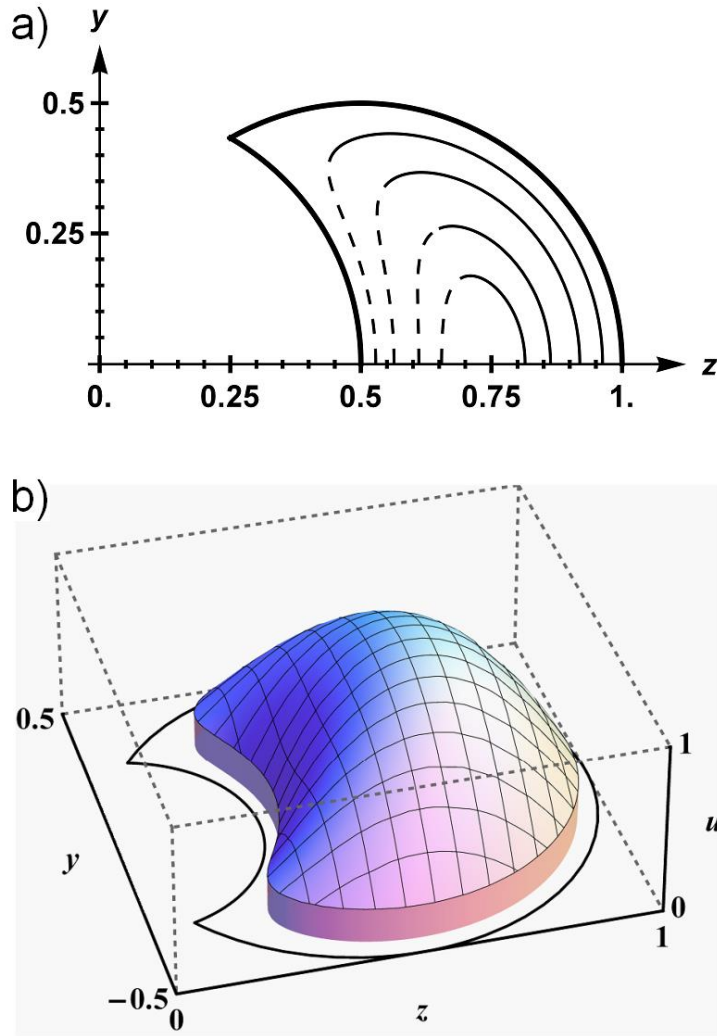
a)

b)

Fig. 4: a) Channel shape (thick solid lines) and position of velocity isolines (thin solid and dashed lines) for $B = 0.5$. The values of the isolines correspond to $\lambda = u / U_{max} = 0.25, 0.5, 0.75, 0.9$ (from outermost to innermost). The solid part of each isoline corresponds to $R_{max,\lambda}$ and the dashed part to $R_{min,\lambda}$ as given by Eq. (31) and Eq. (32), respectively. b) Height function representation of the axial velocity u over the $y - z$ plane for a moon-shaped channel with $B = 0.3$ within area A_λ for $\lambda = 0.5$. The volume below the surface corresponds to the volumetric flow rate $Q(\theta)$ for the specific residence time $\theta = \theta_F / \lambda = 2\theta_F$.
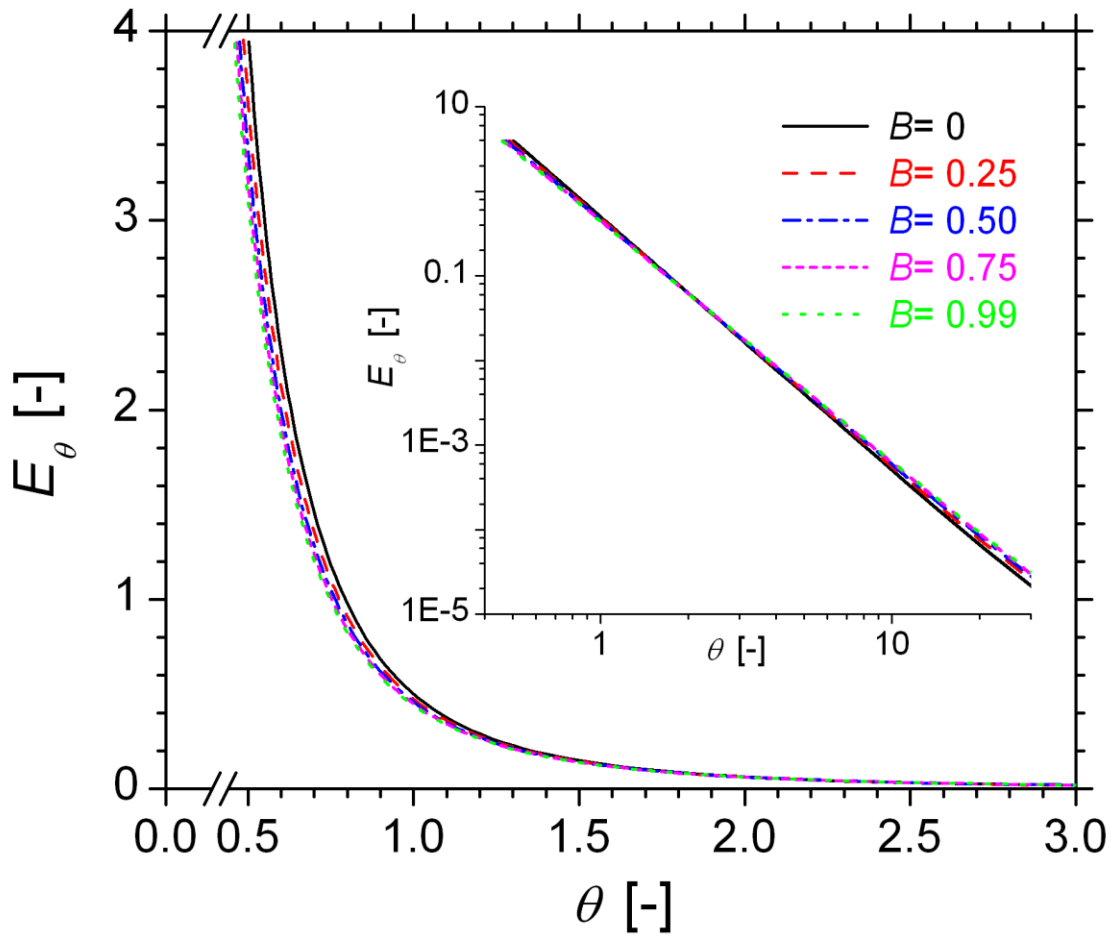
Fig. 5: Differential RTD of moon-shaped channels for $B = 0, 0.25, 0.5, 0.75, 0.99$ in linear and double-log representation. The corresponding channel shapes are shown in Fig. 1 d).
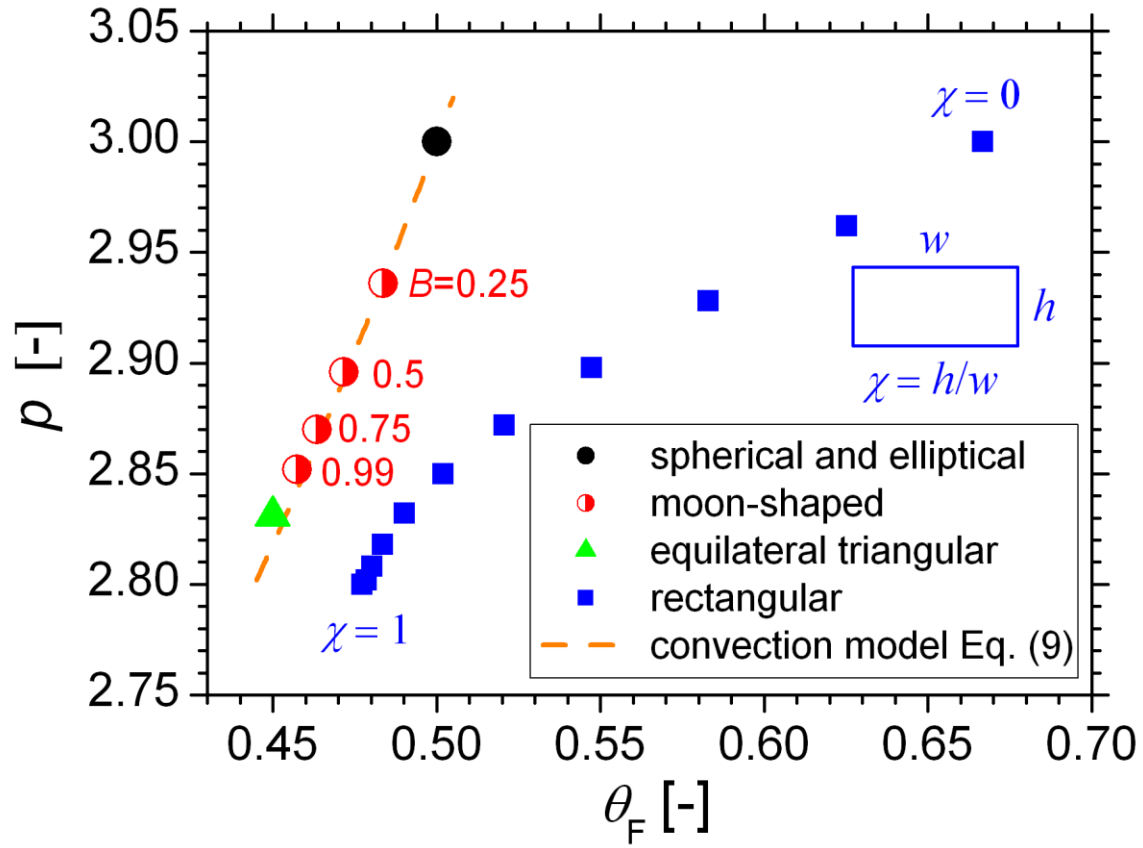
Fig. 6: Parameter p of the generalized two-parameter convection model from Eq. (8) as function of the first appearance time θ_F for different channel shapes (data for rectangular channels are from [12]). The dashed line corresponds to $p = p_{crit} = 2 + (\theta_F^{-1} - 1)^{-1}$ where the two-parameter convection model reduces to the one-parameter convection model of Eq. (9).

Tables

Tab. 1: Values of θ_{F} and p in the generalized two-parameter convection model for moon-shape channels and equilateral triangular channel.

Channel cross-section	θ_{F}	p_{L^2}	$p_{\mathrm{crit}} = 2 + (\theta_{\mathrm{F}}^{-1} - 1)^{-1}$
Moon-shaped with $B = 0.0$ (circular)	0.5000	n.a.	3.000
Moon-shaped with $B = 0.25$	0.4837	2.936	2.937
Moon-shaped with $B = 0.5$	0.4717	2.896	2.893
Moon-shaped with $B = 0.75$	0.4635	2.870	2.864
Moon-shaped with $B = 0.99$	0.4574	2.852	2.843
Equilateral triangular	0.4500	2.831	2.818